INTERNATIONAL JOURNAL FOR NUMERICAL METHODS IN ENGINEERING, VOL. 37, 181–201 (1994)

A FINITE VOLUME FORMAT FOR STRUCTURAL MECHANICS

E. OÑATE, M. CERVERA AND O. C. ZIENKIEWICZ

International Center for Numerical Methods in Engineering, Univ. Politècnica de Cataluña, 08034 Barcelona, Spain

SUMMARY

A general Finite Volume Method (FVM) for the analysis of structural problems is presented. It is shown that the FVM can be considered to be a particular case of finite elements with a non-Galerkin weighting. For structural analysis this can readily be interpreted as equivalent to the unit displacement method which involves mainly surface integrals. Both displacement and mixed FV formulations are presented for static and dynamic problems.

INTRODUCTION

The Finite Volume Method (FVM) evolved in the early seventies via finite difference approximations on non-orthogonal grids. The popularity of the FVM has been extensive in the field of Computational Fluid Dynamics (CFD) and heat transfer.[1–5] On the contrary, in the field of Computational Solid Mechanics (CSM) the use of the FVM has never achieved such acceptance. An early attempt to use FV concepts in CSM is due to Wilkins[6] as an alternative approximation to derivatives in a cell. In this he defines the average gradient of a function u in a volume Ω as

$$\left(\frac{\partial u}{\partial x_i}\right)_\Omega \equiv \frac{1}{\Omega}\int_\Omega \frac{\partial u}{\partial x_i}\,d\Omega = \frac{1}{\Omega}\oint_S u n_i\,ds \tag{1}$$

using the well-known divergence theorem. Such a definition of gradients can be written entirely in terms of function values at the boundary of a volume and has been used in the early 'hydrocodes' of the Lawrence Livermore Laboratory.

The reasons for the unpopularity of the FVM in structural mechanics is understandable, as finite volumes are well known to be less accurate than Galerkin-based finite elements for self-adjoint (elliptic) problems. A comparison between FVM and FEM has been recently presented by Zienkiewicz and Oñate.[7] Here the authors show that FVM and FEM share concepts such as mesh discretization and interpolation, giving precisely the same discretized systems of equations for some particular cases. This coincidence also shows clearly for 2-D and 3-D structural problems as detailed in this work. Here, however, surface integrals are mostly involved and the number of computations can be shown to be proportional to the number of 'sides' in the mesh. This leads to an overall solution cost very similar to that of FE computations (note that for a refined mesh of three-node triangles the number of sides is 1·5 times that of elements). This fact suggests that computational speed is not '*a priori*' one of the keys to the possible success of FVM in structural problems. However, the possibility of obtaining the element matrices and vectors in terms of computations along the element sides opens new possibilities for the solution of some structural problems which, in the authors' opinion, may be worth exploring in detail. Indeed, it

0029–5981/94/020181–21$15.50

Received 23 September 1992
Revised 13 April 1993

appears that substantial storage advantages may be achieved using a side based data structure as shown for some CFD problems.[8]

The layout of the paper is as follows. In the next section a general finite volume format for structural mechanics is presented. Both displacement and mixed formulations are discussed in detail and later on applications to simple bar and Timoshenko beam examples are presented. Finally, possibilities of the FVM for transient dynamic structural problems are discussed and some examples showing the potential of the methods proposed are given.

BASIC EQUATIONS

We consider the solution of the differential equations of linear elastic structural mechanics and their boundary conditions which can be written as[9]

equilibrium equation

$$\mathbf{S}^{\mathrm{T}}\boldsymbol{\sigma} + \mathbf{b}_0 - \rho\ddot{\mathbf{u}} = \mathbf{0} \quad \text{in } \Omega \tag{2}$$

strain definition

$$\boldsymbol{\varepsilon} - \mathbf{S}\mathbf{u} = \mathbf{0} \quad \text{in } \Omega \tag{3}$$

constitutive equation

$$\boldsymbol{\sigma} - \mathbf{D}\boldsymbol{\varepsilon} = \mathbf{0} \quad \text{in } \Omega \tag{4}$$

boundary conditions

$$\mathbf{u} - \mathbf{u}_{\mathrm{p}} = \mathbf{0} \quad \text{in } \Gamma_u \tag{5}$$

$$\mathbf{T}\boldsymbol{\sigma} - \mathbf{t}_{\mathrm{p}} = \mathbf{0} \quad \text{in } \Gamma_t \tag{6}$$

In equations (2)–(6) $\mathbf{u}$, $\boldsymbol{\varepsilon}$ and $\boldsymbol{\sigma}$ are the displacement, stress and strain vectors, respectively, $\mathbf{D}$ is the constitutive matrix, ρ the material density, $\ddot{\mathbf{u}}$ the vector of accelerations, $\mathbf{b}_0$ the constant body forces, $\mathbf{u}_{\mathrm{p}}$ the prescribed displacements at the boundary Γ_u, $\mathbf{t}_{\mathrm{p}}$ the prescribed traction forces at the boundary Γ_t, Ω the domain area or volume with boundary $\Gamma = \Gamma_u \cup \Gamma_t$. Typical examples of matrices $\mathbf{S}$ and $\mathbf{T}$ for 2-D elasticity problems are

$$\mathbf{S} = \begin{bmatrix} \partial/\partial x & 0 \\ 0 & \partial/\partial y \\ \partial/\partial y & \partial/\partial x \end{bmatrix}, \quad \mathbf{T} = \begin{bmatrix} n_x & 0 & n_y \\ 0 & n_y & n_x \end{bmatrix} \tag{7}$$

where n_x, n_y are the components of the unit normal $\mathbf{n}$ to the domain boundary.

Displacement formulation

We will first consider the reduced form of equations (2)–(6) obtained by substituting the strains from equation (3) in equation (4) and the resulting value of the stresses in equations (2) and (6) to give

equilibrium equation

$$\mathbf{S}^{\mathrm{T}}\mathbf{D}\mathbf{S}\mathbf{u} + \mathbf{b}_0 - \rho\ddot{\mathbf{u}} = \mathbf{0} \quad \text{in } \Omega \tag{8}$$

boundary conditions

$$\mathbf{u} - \mathbf{u}_p = \mathbf{0} \quad \text{in } \Gamma_u \tag{9}$$

$$\mathbf{TDSu} - \mathbf{t}_p = \mathbf{0} \quad \text{in } \Gamma_t \tag{10}$$

The weighted residual form of equations (8)–(10) can now be written as

$$\int_\Omega \mathbf{W}^T[\mathbf{S}^T\mathbf{DSu} + \mathbf{b}_0 - \rho\ddot{\mathbf{u}}]\,d\Omega + \int_{\Gamma_u} \mathbf{W}_u^T[\mathbf{u} - \mathbf{u}_p]\,d\Gamma + \int_{\Gamma_t} \mathbf{W}_t^T[\mathbf{TDSu} - \mathbf{t}_p]\,d\Gamma = \mathbf{0} \tag{11}$$

We will now assume that $\mathbf{W}_u = 0$ in Γ_u and that the kinematic boundary conditions (9) are satisfied. Integrating by parts the first term of the first integral in equation (11) and choosing $\mathbf{W}_t = -\mathbf{W}$ yields the well-known expression

$$-\int_\Omega [\mathbf{SW}]^T\mathbf{DSu}\,d\Omega + \int_\Omega \mathbf{W}^T[\mathbf{b}_0 - \rho\ddot{\mathbf{u}}]\,d\Omega + \int_{\Gamma_u} \mathbf{W}^T\mathbf{TDSu}\,d\Gamma + \int_{\Gamma_t} \mathbf{W}^T\mathbf{t}_p\,d\Gamma = \mathbf{0} \tag{12}$$

Remark 1. By choosing now (for 2-D problems) $\mathbf{W}^T = \{\delta u, \delta v\}$, where δu, δv can be interpreted as virtual displacements, equation (12) recovers the usual form of the principle of virtual displacements[9] which can be taken as the starting point for any finite element, or finite volume, formulation.

In *both* FV and FE procedures the independent unknowns are approximated as

$$\mathbf{u} \simeq \hat{\mathbf{u}} = \mathbf{N}_j\bar{\mathbf{u}}_j \quad (j = 1, \ldots, n) \tag{13}$$

where $\bar{\mathbf{u}}_j$ are the unknown parameters and $\mathbf{N}_j$ are the basis functions.[9]

The approximating system of equations (12) is now written as a set of algebraic equations

$$-\int_\Omega [\mathbf{SW}_i]^T\mathbf{DS}\hat{\mathbf{u}}\,d\Omega + \int_\Omega \mathbf{W}_i^T[\mathbf{b}_0 - \rho\ddot{\hat{\mathbf{u}}}]\,d\Omega + \int_{\Gamma_u} \mathbf{W}_i^T\mathbf{TDS}\hat{\mathbf{u}}\,d\Gamma + \int_{\Gamma_t} \mathbf{W}_i^T\mathbf{t}_p\,d\Gamma = \mathbf{0} \tag{14}$$

where $\mathbf{W}_i$ $(i = 1, \ldots, n)$ are now an appropriately selected set of weighting functions.

Equation (14) can be written for linear systems after substitution of the interpolation in equation (13) as

$$\mathbf{M}\ddot{\bar{\mathbf{u}}} + \mathbf{K}\bar{\mathbf{u}} = \mathbf{f} \tag{15}$$

where the usual additive property of element or subdomain contributions is preserved, whatever the form of the weighting functions. In equation (15) **M**, **K** and **f** are, respectively, the mass and stiffness matrices and the equivalent nodal force vector given by

$$\mathbf{M}_{ij} = \int_{\Omega_i} \mathbf{W}_i\rho\mathbf{N}_j\,d\Omega \tag{16a}$$

$$\mathbf{K}_{ij} = \int_{\Omega_i} [\mathbf{SW}_i]^T\mathbf{DSN}_j\,d\Omega - \int_{\Gamma_i} \mathbf{W}_i^T\mathbf{TDSN}_j\,d\Gamma \tag{16b}$$

$$\mathbf{f}_i = \int_{\Omega_i} \mathbf{W}_i^T\mathbf{b}_0\,d\Omega + \int_{\Gamma_{ti}} \mathbf{W}_i^T\mathbf{t}_p\,d\Gamma \tag{16c}$$

In the above, Ω_i is the *control volume* associated with node i (to use finite volume terminology; see Figure 1) where $\mathbf{W}_i \neq \mathbf{0}$. The boundary of the control volume is denoted as Γ_i, excluding the part which may coincide with the external boundary of the total domain where tractions are prescribed; this particular part of the boundary is denoted as Γ_{ti} and it is included in the force

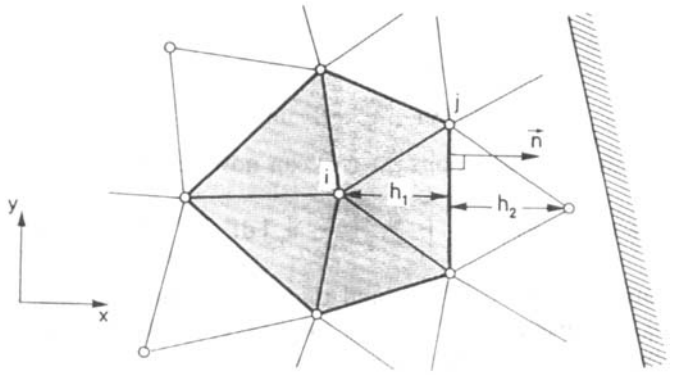

Figure 1. An assembly of finite elements and finite volumes, with shading indicating the control volume

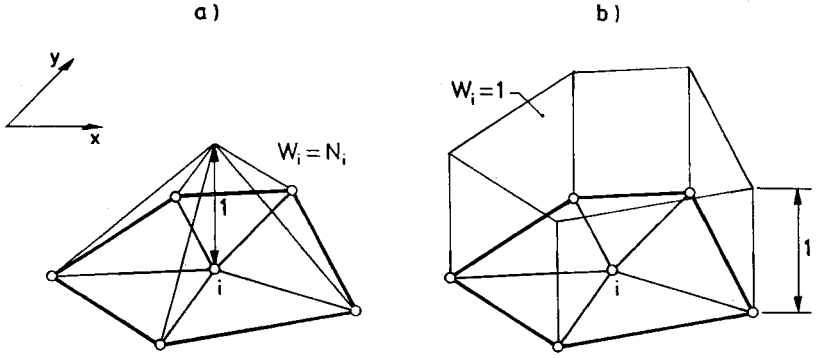

Figure 2. Weighting and basis functions for (a) finite element and (b) finite volume (cell vertex type) approximations for Figure 1.

term. Providing both $\mathbf{W}_i$ and $\mathbf{N}_j$ are chosen so that integrals in equations (16) can be evaluated, then whatever the external boundary, we can specify on it either the tractions ($\mathbf{t}_p$) or the displacements ($\hat{\mathbf{u}} = \mathbf{u}_p$) with equal ease.

Galerkin approach

Structural problems are usually self-adjoint and the optimal weighting is the Galerkin one with $\mathbf{W}_i = \mathbf{N}_i$, thus implying the same approximation for the virtual displacements as that for the actual ones. This leads to minimum energy norm errors and preserves the symmetry of matrices $\mathbf{K}$ and $\mathbf{M}$ (note that the surface integral in equation (16b) now vanishes as N_i is zero at the control volume boundary; see Figure 2a). Hence, the Galerkin approach is the basis of most frequently used finite element procedures. However, other weightings can be used recovering all possible approximation methods.[9] In what follows we shall use standard finite element interpolations $\mathbf{N}_j$ with $\bar{\mathbf{u}}_j$ standing for nodal values in element subdomains.

FINITE VOLUME METHOD

The finite volume procedure is, in fact, a special case of the weighted equation (14) in which

$$\mathbf{W}_i = \mathbf{I} \quad \text{in } \Omega_i, \quad \mathbf{W}_i = 0 \quad \text{elsewhere} \tag{17}$$

where $\mathbf{I}$ is the unity matrix.

Equation (14) can readily be interpreted as applying *unit virtual displacements* over each control volume. Thus, substituting equation (17) into equation (12) yields (as $\mathbf{SI} = \mathbf{0}$)

$$\int_{\Omega_i} \rho \ddot{\hat{\mathbf{u}}}\, d\Omega - \int_{\Gamma_i} \mathbf{TDS}\hat{\mathbf{u}}\, d\Gamma - \int_{\Omega_i} \mathbf{b}_0\, d\Omega - \int_{\Gamma_{ti}} \mathbf{t}_p\, d\Gamma = \mathbf{0} \tag{18}$$

Equation (18) can be written in the standard matrix form of equation (15) using the approximation in equation (13) where now

$$\mathbf{M}_{ij} = \int_{\Omega_i} \rho \mathbf{N}_j\, d\Omega \tag{19a}$$

$$\mathbf{K}_{ij} = -\int_{\Gamma_i} \mathbf{TDSN}_j\, d\Gamma \tag{19b}$$

$$\mathbf{f}_i = \int_{\Omega_i} \mathbf{b}_0\, d\Omega + \int_{\Gamma_{ti}} \mathbf{t}_p\, d\Gamma \tag{19c}$$

In equations (19) definitions of Ω_i, Γ_i and Γ_{ti} coincide with those given for equations (16). We note however that the control volume Ω_i can be prescribed in various ways, and some are discussed in the next sections.

Remark 2. Note that matrix $\mathbf{K}$ of equation (19b) is non-symmetric. However, it can be shown that for the so-called 'cell-centred' FV scheme with a linear approximation the internal force vector (i.e. $\mathbf{K}\bar{\mathbf{u}}$) coincides with that obtained with the standard Galerkin approach (see the appendix). This indicates that a symmetric form of $\mathbf{K}$ identical to that derived from standard FEM can be obtained in this particular case.

Remark 3. Note also the equivalence of the FV approach presented here and the well-known *unit displacement method* in structural mechanics.[10]

Cell vertex scheme

To illustrate the above concepts, consider a field of arbitrary triangles with linear interpolations, with the control volume for the ith node shown shaded in Figure 1. This corresponds in finite volume terminology to the so-called *cell vertex* approach[5] (sometimes quoted as vertex centred approach[9]).

In standard finite element assembly the weighting function $\mathbf{W}_i = \mathbf{N}_i$ is of the form shown in Figure 2(a) and Ω_i includes all the elements associated with the ith node.

Now, if we consider the cell vertex finite volume situation (Figure 2(b)), it is evident that all volume integrals involving derivatives of the constant weighting function disappear. However, a difficulty arises with the boundary integral in the $\mathbf{K}_{ij}$ term of equation (19b), because the displacement gradients involved are not continuous at the interfaces between the elements.

In the normal direction n between two elements, as illustrated in Figure 1, we have a discontinuity shown in Figure 3 with $\partial N_i/\partial n$ jumping from a value $1/h_1$ to $-1/h_2$, where heights of adjacent triangles are denoted as h_1 and h_2.

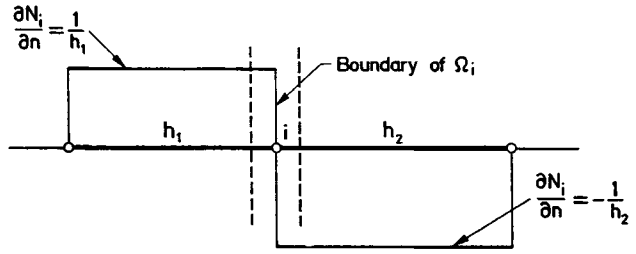

Figure 3. Discontinuity of the gradient at boundaries of control volume

The theory of distributions indicates that the jump in $\partial\hat{u}/\partial n$ across the boundary should be given an average value. It will indeed be found that the mid-value is optimal and then

$$\frac{\partial \hat{u}}{\partial n} = \frac{1}{2}\left(\left.\frac{\partial \hat{u}}{\partial n}\right|_1 + \left.\frac{\partial \hat{u}}{\partial n}\right|_2\right) \tag{20}$$

where $\partial\hat{u}/\partial n|_1$ and $\partial\hat{u}/\partial n|_2$ are, respectively, the values of $\partial\hat{u}/\partial n$ over elements 1 and 2 sharing the interface under consideration.

The jump in $\partial\hat{u}/\partial n$ across the boundaries reflects the discontinuity of tractions along a common boundary in two adjacent elements. This is shown clearly if the first boundary integral in equation (18) is written as $\int_{\Gamma_i} \mathbf{t}\,d\Gamma$, where $\mathbf{t}$ are the tractions acting on the boundary Γ_i.

An illustration of both finite element and finite volume approximations can easily be obtained in the one-dimensional example of a bar of length $2l$ under distributed traction forces, $b(x)$, where equal two-node linear elements of size h are used (see Figure 4).

Here equations (2)–(4) will be written as

$$\begin{aligned} \frac{d}{dx}P + b - \rho A\ddot{u} &= 0 \\ \varepsilon - \frac{d}{dx}u &= 0 \\ P - EA\varepsilon &= 0 \end{aligned} \tag{21}$$

with P the axial force replacing σ, EA the axial stiffness replacing $\mathbf{D}$ and ρA replacing ρ. For simplicity, $EA = k$ = constant and $\rho A = 1$.

The finite element displacement approximation yields a typical assembled equation (which can easily be verified after addition of appropriate integrals) as

$$\frac{h}{6}(\ddot{\bar{u}}_{i+1} + 4\ddot{\bar{u}}_i + \ddot{\bar{u}}_{i-1}) - \frac{k}{h}(\bar{u}_{i+1} - 2\bar{u}_i + \bar{u}_{i-1}) = \int_{-h}^{h} N_i b\,dx \tag{22}$$

The corresponding cell vertex finite volume equation is obtained using the approximations in equations (19)–(20) as

$$\frac{h}{2}(\ddot{\bar{u}}_{i+1} + 2\ddot{\bar{u}}_i + \ddot{\bar{u}}_{i-1}) - \frac{k}{2h}(\bar{u}_{i+2} - 2\bar{u}_i + \bar{u}_{i-2}) = \int_{-h}^{h} b\,dx \tag{23}$$

It can be noted that the two approximations are similar but by no means identical. The finite volume considered has doubled the mass contained in the finite element. The force f_i is also doubled in the case of a *constant* uniformly distributed traction b. Further, the mass is not

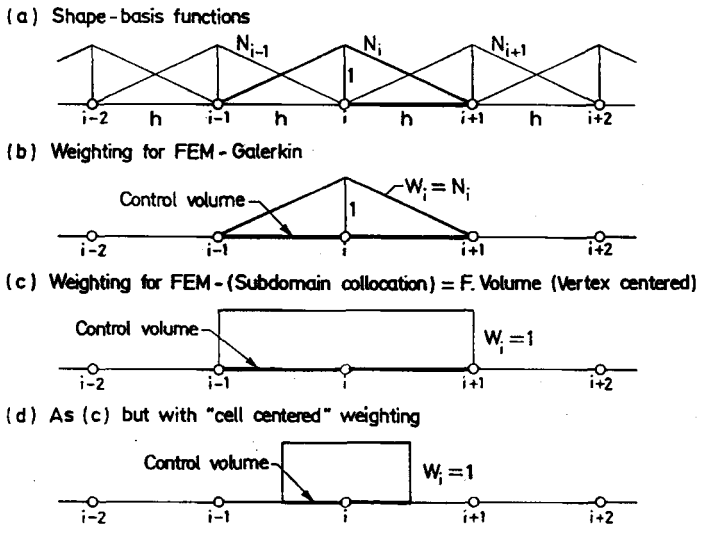

Figure 4. A one-dimensional problem

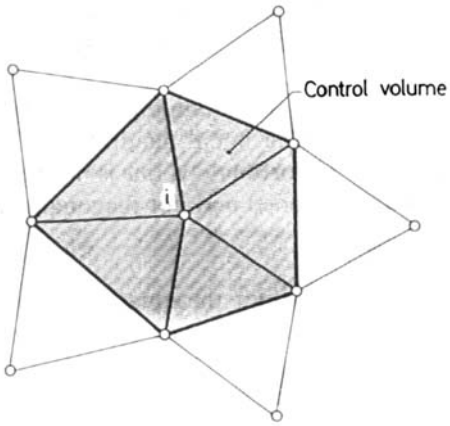

Figure 5. Nodes involved in the discretized equation of an arbitrary control volume using the cell vertex scheme and a 'displacement' formulation

distributed in the same proportion at the nodes and neither is the force when $b = b(x)$. Also, in the FVM the stiffness term is readily recognized as an approximation to *twice* the second derivative of u. This results from using the interface derivatives given by equation (20). It is noticeable that this stiffness term has a wider bandwidth than the one corresponding to the FEM, as it involves external nodes $i - 2$ and $i + 2$. This is an undesirable feature that also occurs in 2-D and 3-D situations, as can be seen in Figure 5. The problem can be overcome by using the so-called *cell centred* schemes, or by avoiding second-order derivatives using a mixed formulation. Both possibilities are discussed in the following sections.

Cell centred finite volume schemes

In the preceding section we have tried to provide 'weighting areas' (i.e. control volumes) coinciding with elements. Clearly, this presents the difficulty of discontinuity of normal derivatives along boundaries and one can now realize why many finite volume methods are applied in so-called *cell centred* schemes. If we consider again the discretization of Figure 1, we can, as in Figure 6, assign a control volume to each node without an overlapping of the weighted area (the obvious division of each triangle is now indicated). In Figure 4 we show the one-dimensional equivalent of this and the reader can easily verify that the finite volume equation now becomes

$$\frac{h}{8}(\ddot{\bar{u}}_{i+1} + 6\ddot{\bar{u}}_i + \ddot{\bar{u}}_{i-1}) - \frac{k}{h}(\bar{u}_{i+1} - 2\bar{u}_i + \bar{u}_{i-1}) = \int_{-h/2}^{h/2} b\,\mathrm{d}x \tag{24}$$

Equation (24) has the same connectivity as the finite element equations and indeed retrieves here exactly the stiffness terms, however showing as before different mass and force distributions.

The use of consistent mass forms, which is found to be beneficial in many transient computations using the finite element approximation, has never found its way into standard finite volume presentation. Here the users invariably lump the masses, implying for instance that equation (24) reads as

$$h\ddot{\bar{u}}_i - \frac{k}{h}(\bar{u}_{i+1} - 2\bar{u}_i + \bar{u}_{i-1}) = \int_{-h/2}^{h/2} b\,\mathrm{d}x \tag{25}$$

It is obvious that if lumping is used, both FE and FV left-hand sides are now identical. If the forces $b(x)$ are constant, both right-hand sides are also identical, and so the systems of equations, for the FVM and the FEM, in this particular case, are the same (and so indeed would be standard finite differences !).

For a cell centred scheme the use of mass lumping is natural, as it can be obtained by integrating the corresponding terms using a nodal quadrature. This very important feature is preserved for 2-D and 3-D situations. Unfortunately, this is not the case for cell vertex schemes, where the mass matrices obtained are banded and not diagonally dominant.

Résumé. We observe at this stage that:

(i) The cell vertex scheme generally 'doubles' the equations as weighting areas are considered repeatedly giving, for instance, in the lumping case a scaled total mass which is not that of the true mass.
(ii) The cell centred scheme, while avoiding the above difficulty, involves complicated element subdivisions.

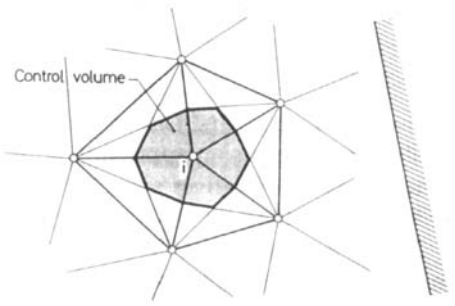

Figure 6. Cell centred control volume

(iii) The second derivatives in the original equation result in interface terms involving gradients on adjacent areas. This, in the case of cell vertex schemes, gives a widening of the equation band over that in standard finite elements.

To avoid this last difficulty we shall next explore the use of mixed formulations in which the starting point is given by first-order equations.

MIXED FINITE VOLUME METHODS

The equilibrium (equation (2)) and constitutive (equation (4)) equations are the starting point for the mixed methods given here, written as

$$\mathbf{S}^{\mathrm{T}}\boldsymbol{\sigma} + \mathbf{b}_0 - \rho\ddot{\mathbf{u}} = \mathbf{0} \tag{26a}$$

$$\mathbf{D}^{-1}\boldsymbol{\sigma} - \mathbf{S}\mathbf{u} = \mathbf{0} \tag{26b}$$

with boundary conditions given by equations (5) and (6).

We now write the weighted residual form of equations (26) and (6) as

$$\int_{\Omega} \mathbf{W}^{\mathrm{T}}[\mathbf{S}^{\mathrm{T}}\boldsymbol{\sigma} + \mathbf{b}_0 - \rho\ddot{\mathbf{u}}]\,\mathrm{d}\Omega + \int_{\Gamma_t} \bar{\mathbf{W}}^{\mathrm{T}}[\mathbf{T}\boldsymbol{\sigma} - \mathbf{t}_{\mathrm{p}}]\mathrm{d}\Gamma = \mathbf{0} \tag{27a}$$

$$\int_{\Omega} \hat{\mathbf{W}}^{\mathrm{T}}[\mathbf{D}^{-1}\boldsymbol{\sigma} - \mathbf{S}\mathbf{u}]\,\mathrm{d}\Omega = \mathbf{0} \tag{27b}$$

In equation (27a) satisfaction of the kinematic boundary conditions $\mathbf{u} = \mathbf{u}_{\mathrm{p}}$ has been assumed Integrating by parts the first term of equation (27a) and making $\bar{\mathbf{W}} = -\mathbf{W}$ yields

$$-\int_{\Omega} (\mathbf{S}\mathbf{W})^{\mathrm{T}}\boldsymbol{\sigma}\,\mathrm{d}\Omega + \int_{\Gamma_u} \mathbf{W}^{\mathrm{T}}\mathbf{T}\boldsymbol{\sigma}\,\mathrm{d}\Gamma + \int_{\Omega} \mathbf{W}^{\mathrm{T}}(\mathbf{b}_0 - \rho\ddot{\mathbf{u}})\,\mathrm{d}\Omega + \int_{\Gamma_t} \mathbf{W}^{\mathrm{T}}\mathbf{t}_{\mathrm{p}}\,\mathrm{d}\Gamma = \mathbf{0} \tag{28}$$

Equations (28) and (27b) are the starting point for both mixed stress–displacement finite element or finite volume approximations.

We will now assume independent interpolations for the displacement and stress fields as

$$\mathbf{u} \simeq \hat{\mathbf{u}} = \mathbf{N}^{u}\bar{\mathbf{u}} \tag{29a}$$

$$\boldsymbol{\sigma} \simeq \hat{\boldsymbol{\sigma}} = \mathbf{N}^{\sigma}\bar{\boldsymbol{\sigma}} \tag{29b}$$

where $\mathbf{N}^{u}$ and $\mathbf{N}^{\sigma}$ are appropriate interpolating functions.

Choosing a finite volume scheme with $\mathbf{W}_i = \mathbf{I}$ over each control volume Ω_i, the following system of discretized equations is obtained:

$$\int_{\Omega_i} \rho\ddot{\hat{\mathbf{u}}}\,\mathrm{d}\Omega - \int_{\Gamma_i} \mathbf{T}\hat{\boldsymbol{\sigma}}\,\mathrm{d}\Gamma - \int_{\Omega_i} \mathbf{b}_0\,\mathrm{d}\Omega - \int_{\Gamma_{ti}} \mathbf{t}_{\mathrm{p}}\,\mathrm{d}\Gamma = \mathbf{0} \tag{30a}$$

$$\int_{\hat{\Omega}_i} \hat{\mathbf{W}}_i^{\mathrm{T}}[\mathbf{D}^{-1}\hat{\boldsymbol{\sigma}} - \mathbf{S}\hat{\mathbf{u}}]\,\mathrm{d}\Omega = \mathbf{0} \tag{30b}$$

where $\hat{\mathbf{W}}_i$ are appropriately selected weighting functions defined over the subdomain $\hat{\Omega}_i$, which need not be identical to Ω_i.

Equations (30) can be written in matrix form, substituting the approximations in equations (29), as

$$\mathbf{M}\ddot{\bar{\mathbf{u}}} - \mathbf{Q}\bar{\boldsymbol{\sigma}} - \mathbf{f} = \mathbf{0} \tag{31a}$$

$$\mathbf{C}\bar{\boldsymbol{\sigma}} - \mathbf{G}\bar{\mathbf{u}} = \mathbf{0} \tag{31b}$$

where

$$\mathbf{M}_{ij} = \int_{\Omega_i} \rho \mathbf{N}_j^u \, d\Omega, \qquad \mathbf{Q}_{ij} = \int_{\Gamma_t} \mathbf{T}\mathbf{N}_j^\sigma \, d\Gamma$$

$$\mathbf{C}_{ij} = \int_{\hat{\Omega}_i} \hat{\mathbf{W}}_i^T \mathbf{D}^{-1} \mathbf{N}_j^\sigma \, d\Omega, \qquad \mathbf{G}_{ij} = \int_{\hat{\Omega}_i} \hat{\mathbf{W}}_i^T \mathbf{S}\mathbf{N}_j^u \, d\Omega \tag{31c}$$

$$\mathbf{f}_i = \int_{\Omega_i} \mathbf{b}_0 \, d\Omega + \int_{\Gamma_{ti}} \mathbf{t}_p \, d\Gamma$$

Matrix $\mathbf{M}$ is, in general, a banded symmetric matrix, while matrix $\mathbf{C}$ is, in general, non-symmetric, thus rendering the solution of equation (30a) computationally difficult. It must again be noted that if a cell centred scheme and a lumping procedure are adopted, matrix $\mathbf{M}$ becomes diagonal. Matrices $\mathbf{Q}$ and $\mathbf{G}$ are rectangular.

Obviously, equation (30b) can be solved separately for each stress component. This implies solving a system of $n \times n$ equations for each stress component (n being the total number of nodes).

The formulation described above is standard for mixed forms and is discussed in some detail in Reference 9, where the usual Galerkin weighting with

$$\mathbf{W} = \mathbf{N}^u \quad \text{and} \quad \hat{\mathbf{W}} = \mathbf{N}^\sigma \tag{32}$$

is used. It is noted, in particular, that for ensuring convergence only certain combinations of $\mathbf{N}^u$ and $\mathbf{N}^\sigma$ are permissible. These are determined by the Babuska–Brezzi requirements or the equivalent *mixed patch test.*[9]

Indeed, for any other weighting functions the same restrictions hold. In the finite volume context we shall use $\mathbf{W}_i = \mathbf{I}$ in Ω_i and $\hat{\mathbf{W}}_i = \mathbf{I}$ in $\hat{\Omega}_i$ and, in general, different collocation subdomains are available for each weighting. In particular, other interesting weighting possibilities exist for equation (31b) and all of them can be explored. Some of these options are discussed in Reference 11. In general, there does not appear to be any advantage in using different weighting subdomains and in the examples to be given later $\Omega_i = \hat{\Omega}_i$.

The use of $\hat{\mathbf{W}}_i = \mathbf{I}$ in $\hat{\Omega}_i$ in equation (30b) leads, for homogeneous material, to the following interesting equation relating the stress within the control volume to the displacements in its boundary:[11]

$$\int_{\hat{\Omega}_i} \mathbf{D}^{-1} \hat{\boldsymbol{\sigma}} \, d\Omega - \int_{\hat{\Gamma}_i} \mathbf{T}^T \hat{\mathbf{u}} \, d\Gamma = \mathbf{0} \tag{33}$$

At this stage it is important to give attention to possible alternatives in choosing $\mathbf{N}^u$ and $\mathbf{N}^\sigma$. An obvious choice is to assume $\mathbf{N}^u$ to be C_0 continuous and $\mathbf{N}^\sigma$ to be elementwise discontinuous. For the cell vertex scheme this will result in equation (30a) being coupled to stresses in neighbouring elements (with the term $\mathbf{T}\boldsymbol{\sigma}$ being taken as an average of the two adjacent values as in equation (20)). However, equation (30b) is strictly determined by the collocation subdomains.

In general, the use of a continuous interpolation for stresses is incorrect if material discontinuities and singularities exist.[9] However, for simple homogeneous cases this can provide accurate results as shown in a later example.

If discontinuous polynomials are used in each element to describe the stress field, then of course correct approximation is achieved, but by the Veubeke equivalence principle[9] the results will be identical to those obtained by a direct displacement approximation, even if the finite volume format is used.

However, if transient solutions are considered and, in particular, if these are used as an iterative process for obtaining steady-state solutions, other possibilities of stress recovery can be used.

Transient explicit solution

Mixed finite volume methods seem particularly well suited for transient explicit problems. The staggered solution of system (31) involves the following steps.

Step 1: displacement computation. Using central differences to discretize equation (31a) in time produces the explicit scheme

$$\bar{\mathbf{u}}^{n+1} = \Delta t^2 \mathbf{M}^{-1}[\mathbf{f}^n - \mathbf{p}_\sigma^n] + 2\bar{\mathbf{u}}^n - \bar{\mathbf{u}}^{n-1} \tag{34}$$

where $\mathbf{M}$ and $\mathbf{f}$ are given by equation (31c), and $\mathbf{p}_{\sigma_i} = -\int_{\Gamma_i} \mathbf{T}\hat{\boldsymbol{\sigma}} \mathrm{d}\Gamma$.

Here, the use of a cell centred scheme with lumped mass matrix is most advantageous, as it only involves vector computations.

Step 2: stress recovery. In the equation

$$\bar{\boldsymbol{\sigma}}^{n+1} = \mathbf{C}^{-1}\mathbf{G}\bar{\mathbf{u}}^{n+1} \tag{35}$$

the different forms of matrices $\mathbf{C}$ and $\mathbf{G}$ discussed in the last section can be used. Clearly, all those resulting in a diagonal $\mathbf{C}$ matrix or leading to direct nodal averaging are computationally advantageous.

We have to note that other procedures can be used for the recovery of nodal stresses, avoiding the use of a finite volume format. In particular, the technique based on local smoothing over element patches of the Gauss point stresses obtained from the displacement values, recently proposed by Zienkiewicz and Zhu,[12,13] provides superconvergent nodal stresses at a relatively low cost and could be an interesting alternative to equation (35). Indeed, such recovery allows both discontinuous and continuous stresses to be obtained as desired and could provide accurate and simple solutions. However, the two-step operation of equations (34) and (35) can be carried out equally in the finite element context and presents no special advantages with finite volumes. We shall therefore consider it separately in another communication. Nevertheless, it is of interest to remark that expressions of the type involved in equation (31a) require only integrals along the boundaries of control volumes in place of area or volume integrals.

SOME NUMERICAL EXAMPLES

In the following we shall consider some examples of finite volume applications to illustrate the type of results obtainable.

Example 1: axially loaded bar—static case

To illustrate the applicability and performance of finite volume methods we shall first consider the simple example of an axially loaded elastic bar (Figure 7). This example has already been discussed for the general dynamic case in a previous section. The axial load b will be taken either as constant (case a: $b = c$) or linear (case b: $b = cx$).

The problem will be solved with both displacement and mixed finite volume formulations using cell vertex and cell centred schemes.

The discretized system of equations for cell vertex and cell centred displacement schemes using a linear interpolation is given by equations (23) and (24), respectively, where acceleration terms are now omitted.

The equivalent mixed equations for the finite volume approximation follow from the general format of equations (30a) and (33) and the particular governing equations (21). We now obtain,

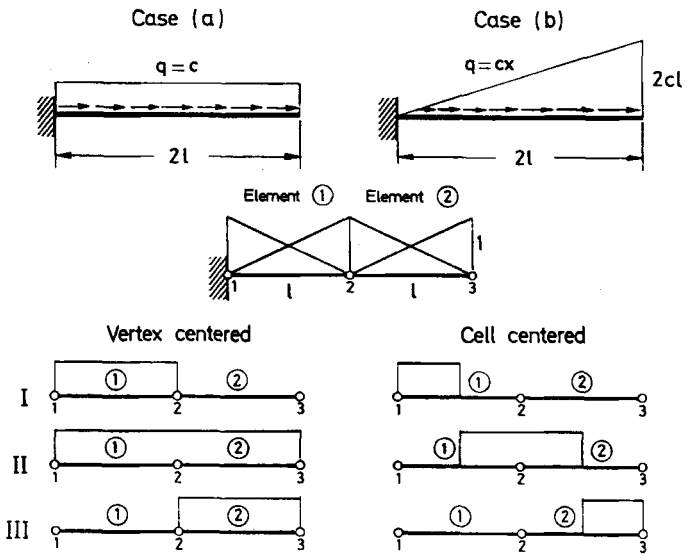

Figure 7. Elastic bar under axial load

omitting acceleration terms, the following general relations with a unit weighting $\mathbf{W}_i = \hat{\mathbf{W}}_i$:

$$P_{\mathrm{R}} - P_{\mathrm{L}} + \int_{l_i} b \, \mathrm{d}x = 0 \tag{36}$$

$$u_{\mathrm{R}} - u_{\mathrm{L}} - \int_{l_i} \frac{P}{k} \, \mathrm{d}x = 0 \tag{37}$$

where the suffixes R and L stand for points on the right and left sides of the control segment. The direct physical interpretation of the above equations is evident, and here lies one of the reasons for the popularity of the finite volumes format.

In detail, for equal sized elements we have the following.

cell vertex solution

$$P_{i+1} - P_{i-1} + \int_{l_i} b \, \mathrm{d}x = 0 \tag{38}$$

$$\frac{h}{2k}(P_{i-1} + 2P_i + P_{i+1}) + u_{i-1} - u_{i+1} = 0 \tag{39}$$

Note that boundary conditions in the end forces values must be imposed in equation (38) only, whereas the displacements are prescribed in equation (39).

cell centred solution

$$P_{i+1} - P_{i-1} + 2\int_{l_i} b \, \mathrm{d}x = 0 \tag{40}$$

$$\frac{h}{4k}(P_{i-1} + 6P_i + P_{i+1}) + u_{i-1} - u_{i+1} = 0 \tag{41}$$

The boundary conditions are treated as mentioned for the cell vertex case.

Two load cases are considered.

Case a: $b = c$. Figure 8 shows the convergence of the cell vertex finite volume solutions for meshes of 1, 2, 3 and 4 elements, respectively. It can be checked that, following the arguments of the previous sections, the cell centred and the finite element solutions for this case are identical and *also* give the exact solution at nodes for *all* meshes.

Case b: $b = cx$. Table I shows the percentage error of the *cell vertex* solution for the nodal axial displacements using three meshes of 1, 2 and 3 elements. Note the large error (50 per cent) in the end displacement obtained with the one-element mesh. This error reduces to 5·55 per cent if three elements are used.

The *cell centred* solution differs in this case from the nodally exact finite element values due to the difference in the nodal load vectors as explained previously. Percentage errors in the nodal displacements for the cell centred case are also presented in Table I and show substantial improvement with respect to the cell vertex solutions.

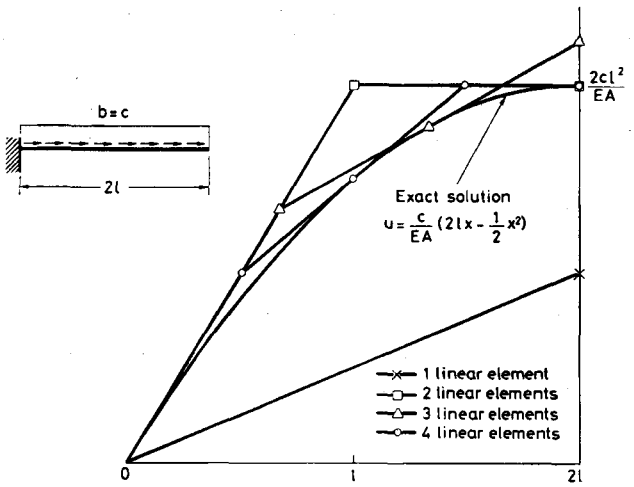

Figure 8. Bar under constant axial load: convergence of FV cell vertex solutions of displacements for different meshes using displacement formulation

Table I. Bar under linearly varying axial load. Percentage errors in nodal displacements for different meshes of linear elements using FE, cell vertex and cell centred FV schemes

		FE		FV/Cell vertex		FV/Cell centered	
Mesh	Node	Displacement (%)	Mixed (%)	Displacement (%)	Mixed (%)	Displacement (%)	Mixed (%)
1-element	2	0·00	0·00	50·0	25·0	12·5	12·5
2-element	2	0·00	9·09	9·09	4·55	2·27	15·9
	3	0·00	0·00	12·5	6·66	3·13	3·13
3-element	2	0·00	0·00	3·85	1·92	0·96	0·96
	3	0·00	4·35	4·35	2·17	1·09	7·61
	4	0·00	0·00	5·55	2·78	1·39	1·39

The second example concerns a mixed finite volume discretization of an equation system for shear coupled so-called Timoshenko beams.

Example 2: Timoshenko beams—mixed finite volume analysis

The equilibrium and constitutive equations for a Timoshenko beam are[9]

$$\begin{aligned} \frac{dM}{dx} + Q &= 0 \\ \frac{dQ}{dx} + q &= 0 \\ \frac{d\theta}{dx} - \frac{M}{EI} &= 0 \\ \left(\frac{dw}{dx} - \theta\right) - \frac{Q}{GA^*} &= 0 \end{aligned} \tag{42}$$

In equations (42), w, θ, M and Q are the vertical displacement, the rotation of the beam sections, the bending moment and the shear force, respectively; E and G are Young's modulus and the shear modulus, I is the inertia of the cross-section and $A^* = \alpha A$, where A is the beam section area and α is the shear correction coefficient ($\alpha = 5/6$ for rectangular sections).

It is well known that the displacement FE formulation for Timoshenko beam elements leads to shear locking unless reduced integration techniques are used.[9] It can easily be checked that the displacement FV approach also exhibits locking. In the FEM this deficiency can be overcome by using a mixed formulation.[9] This is also the case for the FVM, as shown below.

Mixed w–θ–M–Q FV formulation for Timoshenko beams

After adequate weighting and integration by parts of the derivative terms in equations (42) and choosing $W_i = 1$ for all the variables, the following system of equations for the ith volume is obtained:

$$\begin{aligned} M_R - M_L + \int_{l_i} Q\,dx &= 0 \\ Q_R - Q_L + \int_{l_i} b\,dx &= 0 \\ \theta_L - \theta_R + \int_{l_i} \frac{M}{EI}\,dx &= 0 \\ w_L - w_R + \int_{l_i} \theta\,dx + \int_{l_i} \frac{Q}{GA^*}\,dx &= 0 \end{aligned} \tag{43}$$

where again L and R denote the left and right ends of the ith volume. Equations (43) are valid for both cell vertex and cell centred approaches, and again the reader should note the clear physical interpretation of each equation. For the sake of conciseness, we will consider the cell vertex solution only using linear beam elements.

Thus, we will next consider a discretization of the beam of length l in n two-node elements of equal length h (i.e. $nh = l$) with a linear interpolation for all displacement and stress variables. This gives the following system of discretized equations for a generic volume contained between

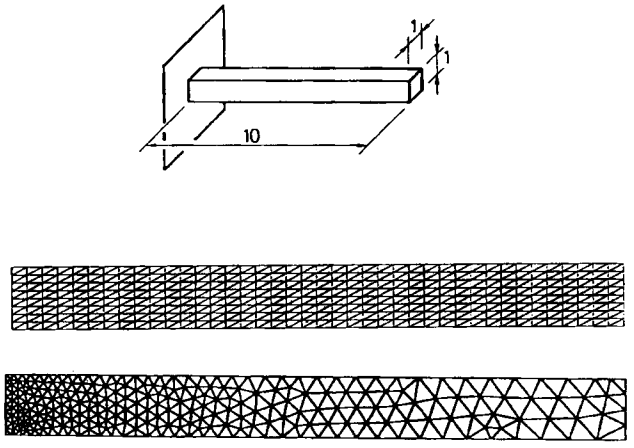

Figure 9. Example 3. Geometry and meshes

nodes $i-1$ and $i+1$:

$$M_{i+1} - M_{i-1} + \frac{h}{2}(Q_{i-1} + 2Q_i + Q_{i+1}) = 0 \tag{44a}$$

$$Q_{i+1} - Q_{i-1} + \int_{l_i} b\,\mathrm{d}x = 0 \tag{44b}$$

$$\theta_{i-1} - \theta_{i+1} + \frac{h}{2EI}(M_{i-1} + 2M_i + M_{i+1}) = 0 \tag{44c}$$

$$w_{i-1} - w_{i+1} + \frac{h}{2}(\theta_{i-1} + 2\theta_i + \theta_{i+1}) + \frac{h}{2GA^*}(Q_{i-1} + 2Q_i + Q_{i+1}) = 0 \tag{44d}$$

Note that the boundary conditions for M, Q, θ and w must be imposed in the appropriate equations.

Equations (44) will now be applied to the analysis of a clamped–free beam under a point load acting at the free end (see Figure 9). It can be shown that the solution using one beam element gives

$$\theta_2 = -\frac{Pl^2}{2EI} \quad \text{(exact)}, \qquad w_2 = -P\left[\frac{l}{GA^*} + \frac{l^3}{4EI}\right] \tag{45}$$

The solution for the end deflection coincides with that obtained with the finite element displacement approach using one-point reduced integration for the shear stiffness terms[9] and differs slightly from the exact value ($w_2 = -P[l/GA^* + l^3/3EI]$). Table II shows the convergence of the end deflection values obtained with meshes of 1, 2 and 3 linear beam elements. Note that the end rotation obtained is exact for all the meshes.

In Reference 11 the authors have also investigated the use of a three-field w–θ–Q mixed FV approach for this problem. Numerical results for this case also show the absence of locking, as expected, although some accuracy is lost for the end rotation values.

Example 3: transient 2-D elasticity

To illustrate the applicability and performance of FV methods in the context of transient 2-D elasticity, we shall consider a simple example of an elastic bar of dimensions $10 \times 1 \times 1$ under

Table II. End deflection values for a clamped–free beam under a point load acting at the free end (mixed w–θ–M–Q cell vertex formulation)

Exact	$w = -P\left[\frac{l}{GA^*} + \frac{l^3}{3EI}\right]$	$\theta = -P\frac{l^3}{2EI}$
1 element	$w = -P\left[\frac{l}{GA^*} + \frac{l^3}{4EI}\right]$	End rotation exact
2 elements	$w = -P\left[\frac{l}{GA^*} + \frac{l^3}{\frac{16}{5}EI}\right]$	End rotation exact
3 elements	$w = -P\left[\frac{l}{GA^*} + \frac{l^3}{\frac{108}{35}EI}\right]$	End rotation exact

plane stress conditions (Figure 9). The material properties selected are: Young's modulus $E = 1{\cdot}0 \times 10^{-2}$, Poisson's ratio $\nu = 0{\cdot}1$ and density $\rho = 1{\cdot}0$. Two cases will be considered in which loads are suddenly applied as: (i) constant body forces $\mathbf{b}_0$ acting in the direction of the bar, and (ii) constant body forces $\mathbf{b}_0$ acting in the direction normal to the bar. Case (i) is, in fact, a one-dimensional stress wave propagation problem if the Poisson's effect is neglected. Case (ii) is a free oscillation problem under lateral load.

The problem will be solved with both displacement and mixed finite volume formulations using cell centred schemes, which provides naturally a lumped mass matrix. In both, the explicit format of solution given in equations (34) and (35) is applied. For comparison, both mixed and displacement finite element models have been used.

Three mesh subdivisions have been used, two of which are shown in Figure 9:

(1) Structured fine: $80 \times 8 \times 2$ CST elements (729 nodes, 2008 sides)
(2) Structured coarse: $40 \times 4 \times 2$ CST elements (205 nodes, 524 sides)
(3) Unstructured: 444 CST elements (268 nodes, 711 sides)

Case (i): body forces in the direction of the bar. The results obtained for the end deflection using mesh (1) with both FV and FE (with lumped mass) displacement methods are plotted in Figure 10. For the displacement format, results are of course identical for both methods, as the body loads are constant. It can be proved that also for the mixed formulation, FV and FE results are approximately the same for constant body loads and, in fact, they coincide exactly if an additional approximation is admitted when performing the appropriate boundary integrals in the FVM (see equation (54) in the appendix). The results for the mixed method overlap with those plotted in Figure 10.

Case (ii): body forces normal to the bar. Figure 11(a) shows the end deflection of the bar using meshes (1), (2) and (3), and the FV displacement method. It has to be remarked that these results are identical to those provided by the FEM, as the load is constant. Moreover, the unstructured mesh achieves almost the same accuracy as the fine regular mesh at nearly one-third of the CPU cost. The thin beam theory exact solution has a peak deflection of 3·0.

Figure 11(b) shows the end deflection of the bar using meshes (1), (2) and (3), and the FV mixed method, with linear interpolation for both displacements and stresses. It has to be pointed out

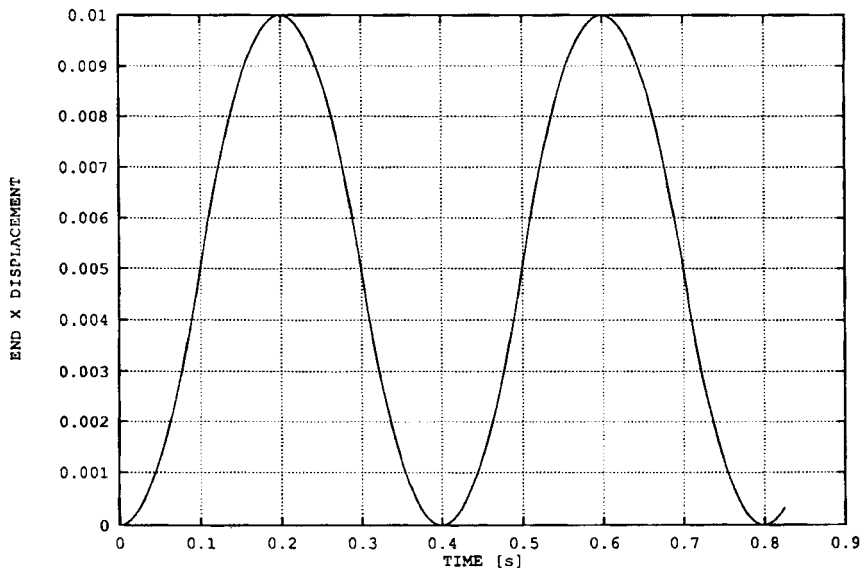

Figure 10. Bar under longitudinal body forces: end deflection using displacement formulation and mesh (1); both FV and FE results coincide

Table III. CPU time comparison between the different formulations for case (ii) (fine mesh)

Formulation	Total CPU time(s)	Internal forces evaluation CPU time(s)	Stress evaluation CPU time(s)
Displacement-FEM	474·39	242·87	133·57
Displacement-FVM	508·75	277·12	134·13
Mixed-FEM	763·91	294·88	370·39
Mixed-FVM	880·19	412·42	363·70

again that these results are equal to those provided by the mixed FEM, as the load is constant, and the approximation described in the appendix has been used. Remembering that the thin beam theory exact solution has a peak deflection of 3·0, it is remarkable to see that the mixed method provides a convergent solution with larger displacements than the exact solution. The results show again how the unstructured mesh achieves almost the same accuracy as the fine regular mesh with one-third of the CPU cost.

Finally, Table III shows the comparison between the CPU times spent for the solution of problem 3(ii) using the different formulations (for the fine mesh). The problem has been run in a CONVEX C-120 machine (one vectorial processor). It can be seen that the displacement formulations are far less costly than the mixed ones, due to the fact that they only require the solution of one set of equations. CPU time comparison between FEM and FVM is favourable to the first, but only slightly for the irreducible case.

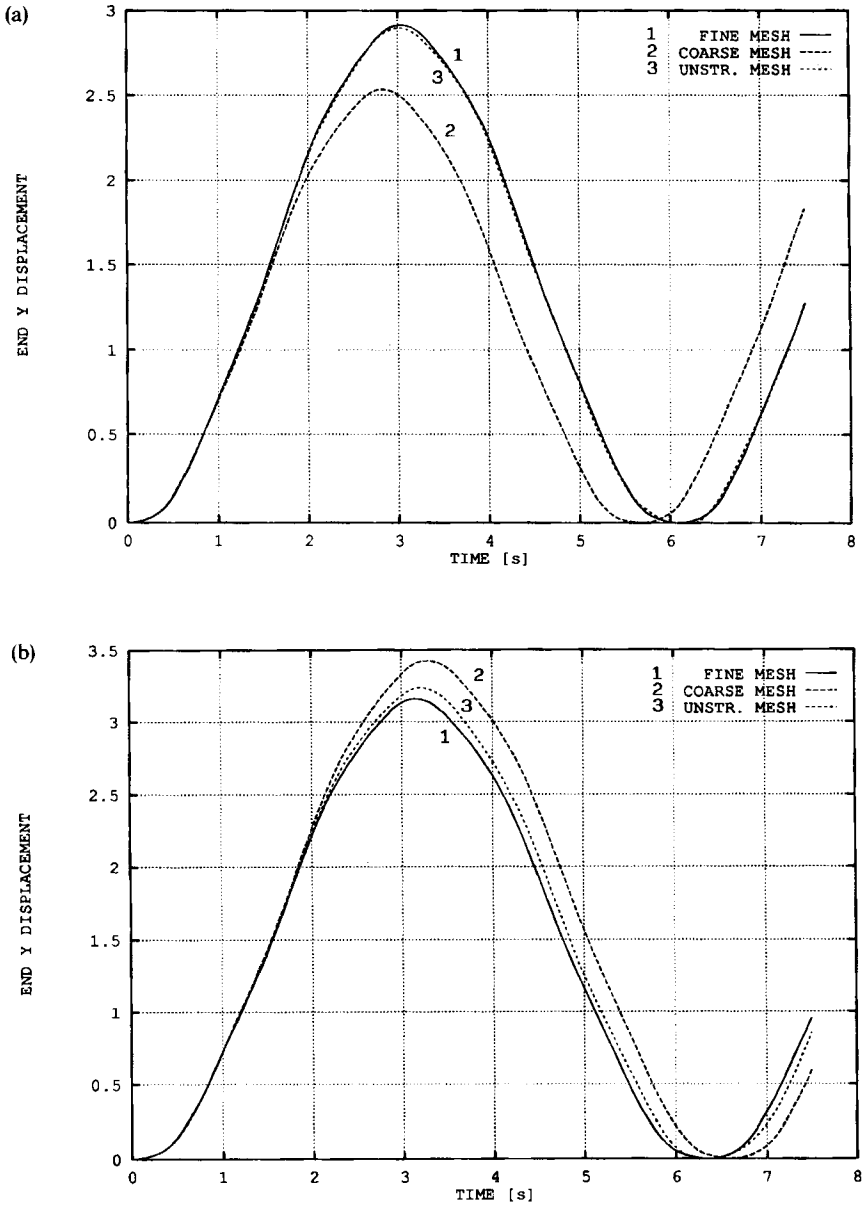

Figure 11. Bar under transversal body forces: end deflection using (a) displacement formulation and (b) mixed formulation for meshes (1), (2) and (3); FV and FE results coincide in all cases

CONCLUSIONS

The FVM is presented in a format applicable to structural mechanics. It is shown that the FVM can be considered as a particular case of finite elements with a non-Galerkin weighting, equivalent to the use of a constant virtual displacement field. The resulting equations are identical to those provided by the well-known unit displacement method.

The displacement FVM is discussed and both cell vertex and cell centred schemes have been examined. Cell centred schemes are preferable because they provide naturally diagonal mass matrices and the internal force terms as the FEM. Thus, for constant body forces the FE and FV solutions are identical.

The mixed FVM has also been discussed, with different options for the weighting of the constitutive equation. Again, cell centred schemes are preferable because they provide naturally diagonal matrices for both equations. It is shown that weighted nodal averaging of stresses is a simple and valid alternative. Explicit transient analysis is presented in this context, both by its intrinsic interest and as an iterative procedure to solve static problems.

Example 1 proves that the cell centred scheme is more accurate than the cell vertex scheme for the simple problem presented. Also, the benefits of a mixed formulation are underlined.

Example 2 shows the possibilities of mixed FVM for bending problems, as the two schemes proposed are convergent and present no locking, as expected.

Example 3 shows the possibilities of displacement and mixed FVM in plane elasticity. It is demonstrated that under constant loads, FV and FE approximations produce *exactly* the same systems of equations, and thus the same results for the irreducible formulation. This is also the case for the mixed formulation if an additional approximation is admitted when performing the appropriate boundary integrals.

It seems that the merits of the FVM could lie in the storage advantage provided by using a side based data structure and also in the possibility of computing element matrices and vectors using boundary integrals along the control volume sides, involving information provided by adjacent elements. These features are currently under investigation by the authors.

ACKNOWLEDGEMENT

The authors wish to express their gratitude to Dr. R. Codina for his useful comments during the realization of this work.

APPENDIX

It was stated in Example 3 that both FV (cell centred scheme) and FE approximations produce the same internal force terms for the displacement and mixed formulations when three-noded linear elements are used. That is to say, the vectors

$$\mathbf{p}_\sigma^{\mathrm{FE}} = \int_{\Omega_i} (\mathbf{SN})^{\mathrm{T}} \boldsymbol{\sigma}\, \mathrm{d}\Omega \tag{46}$$

$$\mathbf{p}_\sigma^{\mathrm{FV}} = -\int_{\Gamma_i} \mathbf{T}\boldsymbol{\sigma}\, \mathrm{d}\Gamma \tag{47}$$

are identical component by component.

Let us first consider the *displacement formulation*. The kth component of the ith node of the internal force vector for FE is (from (46) and using tensor notation for the stresses)

$$p_{ik}^{\mathrm{FE}} = \int_{\Omega_i} \frac{\partial N_i}{\partial x_j} \sigma_{jk}\, \mathrm{d}\Omega = \sum_{e=1}^{n_{\mathrm{el}}} \int_{\Omega_i^e} \frac{\partial N_i^e}{\partial x_j} \sigma_{jk}^e\, \mathrm{d}\Omega = \sum_{e=1}^{n_{\mathrm{el}}} \sigma_{jk}^e \int_{\Omega_i^e} \frac{\partial N_i^e}{\partial x_j}\, \mathrm{d}\Omega \tag{48}$$

for a patch of n_{el} elements concurrent at node i (Figure 12).

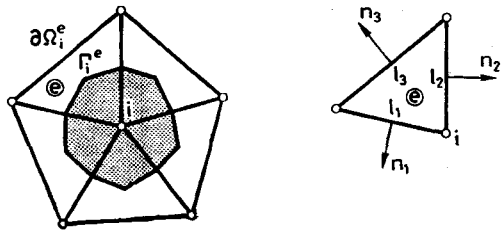

Figure 12. A patch of elements concurrent at the ith node

On the other hand, the kth component of the ith node of the internal force vector for FV is (from (47))

$$p_{ik}^{\mathrm{FV}} = -\int_{\Gamma_i} n_j \sigma_{jk} \mathrm{d}\Gamma = \sum_{e=1}^{n_{el}} -\int_{\Gamma_i^e} n_j \sigma_{jk}^e \mathrm{d}\Gamma = \sum_{e=1}^{n_{el}} \sigma_{jk}^e \left(-\int_{\Gamma_i^e} n_j \mathrm{d}\Gamma \right) \tag{49}$$

But, for the eth element, with sides of length l_1, l_2, l_3 and external unit normals $\mathbf{n}_1, \mathbf{n}_2, \mathbf{n}_3$, respectively (see Figure 12), we can write

$$\int_{\Omega_i^e} \frac{\partial N_i^e}{\partial x_j} \mathrm{d}\Omega = \int_{\partial\Omega_i^e} n_j N_i^e \mathrm{d}\Gamma = n_{1j} \tfrac{1}{2} l_1 + n_{2j} \tfrac{1}{2} l_2 = -n_{3j} \tfrac{1}{2} l_3 = -\int_{\Gamma_i^e} n_j \mathrm{d}\Gamma \tag{50}$$

where $\partial\Omega_i^e$ is the complete boundary of element e, while Γ_i^e is the part of the boundary of the cell Ω_i *interior* to element e.

With the result from (50) the identity $p_{ik}^{\mathrm{FE}} = p_{ik}^{\mathrm{FV}}$ is demonstrated.

Let us now consider the *mixed formulation* with linear interpolations for both displacements and stresses:

The kth component of the ith node of the internal force vector for FE is (from (47))

$$p_{ik}^{\mathrm{FE}} = \int_{\Omega_i} \frac{\partial N_i}{\partial x_j} \sigma_{jk} \mathrm{d}\Omega = \sum_{e=1}^{n_{el}} \int_{\Omega_i^e} \frac{\partial N_i^e}{\partial x_j} \sigma_{jk}^e \mathrm{d}\Omega = \sum_{e=1}^{n_{el}} \int_{\Omega_i^e} \frac{\partial N_i^e}{\partial x_j} \left(\sum_{r=1}^{3} N_r^e \sigma_{jk}^r \right) \mathrm{d}\Omega \tag{51}$$

The shape functions N_r being linear, this integral can be evaluated using the values of σ_{jk} at the centroid of the triangle, i.e.

$$\bar{\sigma}_{ij}^e = \frac{1}{3} \sum_{r=1}^{3} \sigma_{jk}^r \tag{52}$$

and then

$$p_{ik}^{\mathrm{FE}} = \sum_{e=1}^{n_{el}} \bar{\sigma}_{jk}^e \int_{\Omega_i^e} \frac{\partial N_i}{\partial x_j} \mathrm{d}\Omega \tag{53}$$

On the other hand, the kth component of the ith node of the internal force vector for FV is (from (47))

$$p_{ik}^{\mathrm{FV}} = -\int_{\Gamma_i} n_j \sigma_{jk} \mathrm{d}\Gamma = \sum_{e=1}^{n_{el}} -\int_{\Gamma_i^e} n_j \left(\sum_{r=1}^{3} N_r^e \sigma_{jk}^r \right) \mathrm{d}\Gamma \simeq \sum_{r=1}^{n_{el}} \bar{\sigma}_{jk}^e \left(-\int_{\Gamma_i^e} n_j \mathrm{d}\Gamma \right) \tag{54}$$

Note that the last step in (54) is an approximation, as the stresses σ_{jk}^e are linear inside the element.

Comparing (51) with (54), and using the result from (50), the expression $p_{ik}^{\mathrm{FE}} \simeq p_{ik}^{\mathrm{FV}}$ is demonstrated.

REFERENCES

1. P. W. MacDonald, 'The computation of transonic flow through two dimensional gas turbine cascades', *ASME Paper 71-GT-89*, 1971.
2. R. W. MacCormack and A. J. Paullay, 'Computational efficiency achieved by time splitting of finite difference operators', *AIAA 72-154*, San Diego, 1972.
3. A. W. Rizzi and M. Inouye, 'Time split finite volume method for three dimensional blunt-body flows', *AIAA J.*, **11**, 1478–1485 (1973).
4. S. V. Patankar, in W. J. Minkowycz and E. M. Sparrow (eds.), *Numerical Heat Transfer and Fluid Flow*, Series in Computational Methods in Mechanics and Thermal Sciences, Hemisphere, Washington, DC, 1980.
5. C. Hirsch, *Numerical Computation of Internal and External Flow*, Vol. I, Wiley, New York, 1989.
6. M. L. Wilkins, 'Calculations of elasto-plastic flow', in Balder *et al.* (eds.), *Methods of Computational Physics*, Vol. 3, Academic Press, New York, 1964.
7. O. C. Zienkiewicz and E. Oñate, 'Finite elements versus finite volumes. Is there really a choice?', in P. Wriggers and W. Wagner (eds.), *Nonlinear Computation Mechanics. State of the Art*, Springer, Berlin, 1991.
8. J. Peraire, J. Peiró and K. Morgan, 'A 3D finite element multigrid solver for the Euler equations', AIAA Aerospace Sciences Meeting, Reno, 1992.
9. O. C. Zienkiewicz and R. L. Taylor, *The Finite Element Method*, McGraw-Hill, New York, 1989 (Vol. I), 1991 (Vol. II).
10. R. H. Gallagher, 'A correlation study of matrix structural analysis', *AGAR Dograph 69*, Pergamon Press, Oxford, 1964.
11. E. Oñate, M. Cervera and O. C. Zienkiewicz, 'A study of the finite volume method for structural mechanics', *Internal Report Publication No. 15*, CIMNE, Barcelona, 1992.
12. O. C. Zienkiewicz and J. Z. Zhu, 'Superconvergent derivative recovery techniques and *a posteriori* error estimations in the finite element method. Part I: a general superconvergent recovery technique', *Internal Report CR/671/91*, Univ. Coll. of Swansea, 1991; *Int. j. numer. methods eng.*, to be published.
13. O. C. Zienkiewicz and J. Z. Zhu, 'Superconvergent derivative recovery techniques and *a posteriori* error estimations in the finite element method. Part I: the Zienkiewicz–Zhu *a posteriori* error estimator', *Internal Report CR/672/91*, Univ. Coll. of Swansea, 1991; *Int. j. numer. methods eng.*, to be published.
14. G. Cantin, G. Loubignac and G. Touzot, 'An iterative algorithm to build continuous stress and displacement solutions', *Int. j. numer. methods eng.*, **12**, 1493–1506 (1978).